JTTEE5 15:481-487
DOI: 10.1361/105996306X147126
1059-9630/$19.00 © ASM International

Technical Note

Simulation of Particle-Shock Interaction in a High Velocity Oxygen Fuel Process

V.R. Srivatsan and A. Dolatabadi

(Submitted March 2, 2006; in revised form July 14, 2006)

High velocity oxygen fuel process (HVOF) involves supersonic two-phase flow of gas-solid particles. Two kinds of shocks are formed in a typical high velocity oxygen fuel process. Adjustment of the overexpanded flow to the atmospheric pressure at the exit of the nozzle results in formation of shock diamonds while high speed flow impingement on a substrate creates bow shock. The latter is found to be responsible for deviation of the injected particles from their trajectories near the substrate, which significantly reduces the chance of some particles landing on the substrate. An attempt is made to study the behavior of particle trajectory as it interacts with the bow shock formed near the substrate. The strength and location of bow shock was found to vary for different substrate geometries and standoff distances. In this work, various particle sizes impinging on substrates with various configurations (flat, concave, and convex) are simulated and the effect of shock diamonds and bow shock on particle trajectory is studied.

Keywords bow shock, high velocity oxygen fuel, particle conditions, particle-interaction, shock diamonds, substrate configuration

1. Introduction

Thermal spray coatings are formed by the impingement of a stream of molten or semi-molten particles on a substrate. One of the most commonly used thermal spray technologies is high velocity oxygen fuel (HVOF) process in which combustion of a mixture of fuel and oxygen accelerates the coating particles fed inside a converging–diverging nozzle. A schematic of an HVOF process is shown in Fig. 1. The combustion of gases gives raise to relatively high temperature of about 2200 °C and high pressure of about 4 atm. The pressure and temperature profile of an HVOF process is given in Fig. 2(a) and 2(b), respectively. The injected particles on interaction with the gas phase attain high velocity (above 500 m/s) at relatively low temperature, thereby gaining high kinetic and thermal energy. High kinetic energy of coating particles upon impact leads to the formation of a well adhered coating on the substrate.

One of the goals of any thermal spray process is to attain high deposition efficiency. Deposition efficiency is defined as the ratio of mass of particles deposited on a substrate to the mass of particles fed to the nozzle. In general, the deposition efficiencies of thermal spray systems are not satisfactory. From 20 up to 55% of the particles fed to a spray gun escape from the field and are not deposited on the substrate (Ref 1). This is mainly due to particles that have a very low normal velocity upon impact on the substrate (Ref 2). There are many factors that affect this deposition efficiency like nozzle geometry, gas flow conditions, mass flow rate of particles, particle normal velocity to the surface of the substrate upon impingement, and substrate configuration (Ref 3).

In this work, we have attempted to study the effect of geometry of the substrate and substrate standoff distance on deposition efficiency by analyzing the gas flow and the trajectory of particles of various sizes and their impact velocity near the substrate. The over-expanded gas flow at the nozzle exit would undergo series of compressions and expansions giving raise to shock diamonds. In addition, the presence of substrate decelerates the gas velocity significantly, giving rise to strong bow shocks, which form on the surface of the substrate. These shocks cause the particles to deviate from their trajectories, which makes those particles' chances of impingement on the substrate questionable. The nature of shock diamonds and bow shocks are strongly dependent on substrate standoff distance and substrate configuration. We have compared the flow pattern near the substrate of three different shapes (i.e., flat, concave, and convex). Additionally, the trajectory of the particles of different sizes and their deposition characteristic on the previously mentioned substrates were examined.

2. Methodology

High velocity oxygen fuel process usually involves supersonic viscous turbulent flow with solid particles. To capture the characteristics of the gas-solid particles flow, a compressible two-phase flow analysis is required. The governing equations are solved for the gas phase in an Eulerian frame, and equation of

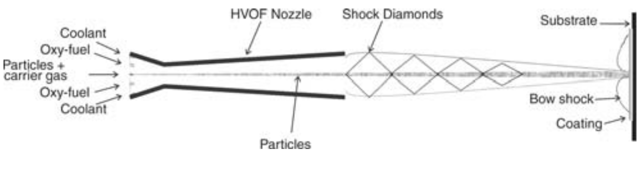

Fig. 1 Schematic of an HVOF process

This article was originally published in *Building on 100 Years of Success, Proceedings of the 2006 International Thermal Spray Conference* (Seattle, WA), May 15-18, 2006, B.R. Marple, M.M. Hyland, Y.-Ch. Lau, R.S. Lima, and J. Voyer, Ed., ASM International, Materials Park, OH, 2006.

V.R. Srivatsan and **A. Dolatabadi,** Department of Mechanical and Industrial Engineering, Concordia University, Montreal, Canada. Contact e-mail: dolat@encs.concordia.ca.

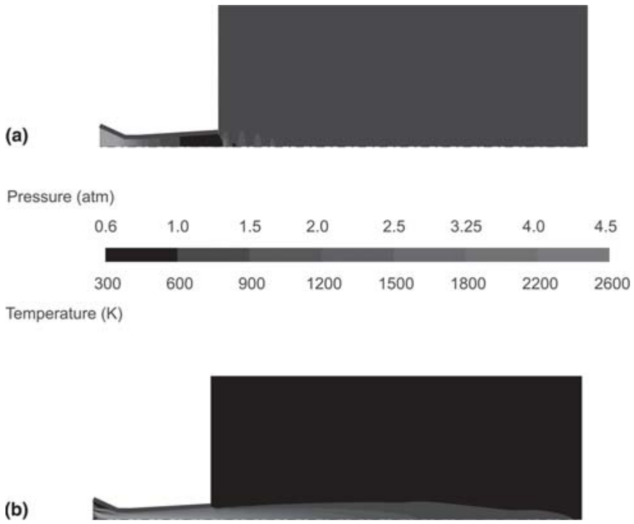

Fig. 2 Pressure and temperature profile of a typical HVOF process

Table 1 Chemical reaction for modeling combustion and their respective enthalpy of reaction

Reaction steps	Chemical reaction	Enthalpy of reaction, kJ/kg · mol
1.	$C_3H_6 + \frac{1}{2}O_2 \rightarrow 3CO + 3H_2$	-3.5126×10^5
2.	$CO + \frac{1}{2}O_2 \rightarrow CO_2$	-2.8317×10^5
3.	$H_2 + \frac{1}{2}O_2 \rightarrow H_2O$	-2.4190×10^5

Table 2 Mass flow rate of fluids used in simulation

Inlet	Species	Mass flow rate, kg/s
1	N_2 (Carrier gas)	1.573×10^{-4}
	MCrAlY particles	5.400×10^{-4}
2	C_3H_6	2.256×10^{-3}
	O_2	6.484×10^{-3}
3	N_2 (Coolant)	8.604×10^{-3}

motion for a solid particle in the Lagrangian framework. Inert solid spherical particles are modeled, and a uniform temperature distribution inside each particle is considered (lumped capacitance system). The first three steps of the chemical reactions used in (Ref 4) are used to model the combustion. The chemical reactions used to model the combustion are given in Table 1.

2.1 Governing Equation

2.1.1 Gas Phase. The governing equations for the gas phase are the continuity, momentum, energy, and ideal gas state equations for viscous, compressible, and turbulent flow. The equations are expressed in Cartesian tensor form with the Einstein summation convention:

2.1.2 Continuity Equation.

$$\frac{\partial \rho}{\partial t} + \frac{\partial(\rho u_j)}{\partial x_j} = 0 \qquad \text{(Eq 1)}$$

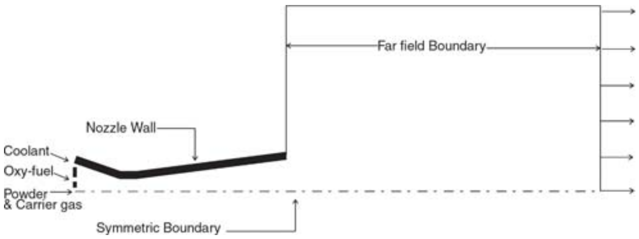

Fig. 3 Boundary condition and computational domain for the numerical simulation

2.1.3 Momentum Equation.

$$\frac{\partial}{\partial t}(\rho u_i) + \frac{\partial}{\partial x_j}(\rho u_j u_i) = -\frac{\partial p}{\partial x_i} + S_{u_i} + \frac{\partial}{\partial x_j} \left\{ \mu_{\text{eff}} \left(\frac{\partial u_i}{\partial x_j} + \frac{\partial u_j}{\partial x_i} \right) - \frac{2}{3}\mu_{\text{eff}} \frac{\partial u_l}{\partial x_l} \delta_{ij} \right\} \qquad \text{(Eq 2)}$$

2.1.4 Energy Equation.

$$\frac{\partial}{\partial t}(\rho H) + \frac{\partial}{\partial x_j}(\rho u_j H) - \frac{\partial p}{\partial t} = \frac{\partial}{\partial x_j}\left(\lambda \frac{\partial T}{\partial x_j} + \frac{\mu_t}{\text{Pr}_t}\frac{\partial h}{\partial x_j} \right) + S_E + \frac{\partial}{\partial x_j}\left\{ u_j \left[\mu_{\text{eff}} \left(\frac{\partial u_i}{\partial x_j} + \frac{\partial u_j}{\partial x_i} \right) - \frac{2}{3}\mu_{\text{eff}} \frac{\partial u_l}{\partial x_l}\delta_{ij} \right] + \mu \frac{\partial k}{\partial x_j} \right\} \qquad \text{(Eq 3)}$$

where $\mu_{\text{eff}} = \mu + \mu_t$, $H = h + \frac{1}{2}(u_i u_i) + k$, λ, k, and S are effective viscosity, total enthalpy, thermal conductivity, turbulent kinetic energy, and source terms, respectively. The standard k-ε turbulence model of Launder and Spalding (Ref 5) is considered, where k is the turbulent kinetic energy and ε is the rate of its dissipation.

2.2 Particle Phase

The motion of each particle in the gas-particle flow is modeled by the Lagrangian particle tracking method. Two-way coupling between the gas and particulate phases is provided by source terms in the momentum and energy equations, which include the effect of particulate phase on the gas phase. The equation of motion for a particle in the gas flow is (Ref 6)

$$m_p \frac{d\vec{U}_p}{dt} = \frac{1}{2}\rho_g A_p C_D (\vec{U}_g - \vec{U}_p)\left|\vec{U}_g - \vec{U}_p\right| + \vec{F} \qquad \text{(Eq 4)}$$

where m_p is the mass of particle, U_p and U_g are instantaneous particle and gas velocities, respectively. ρ_g is the gas density, A_p is the particle cross-sectional area, and F denotes external forces such as gravitational force. Integrating the previous equation of motion for a particle results in the particle velocity. A second integration over the time interval will result in the particle position. Drag coefficient of the particle plays an important role in momentum transfer between the gas and solid particle phases. As our case involves very high velocities, we have used the C_D correlation given by Eq 5, which is appropriate for supersonic velocities and high temperatures (Ref 7). In this correlation compressibility effects are considered using particle Mach number defined as the ratio of relative velocity of the gas and particle to the velocity of sound.

$$C_D = \begin{cases} 24\left(\mathrm{Re}_p + (\gamma/2)^{1/2}\,Ma_p\left\{4.33 + \left(\dfrac{3.65 - 1.53T_p/T}{1 + 0.353T_p/T}\right)\exp\left[-0.247(2/\gamma)^{1/2}\dfrac{\mathrm{Re}_p}{Ma_p}\right]\right\}\right)^{-1} & \\ + \exp\left(-\dfrac{0.5\,Ma_p}{\mathrm{Re}^{1/2}}\right)\left[\dfrac{4.5 + 0.38(0.03\,\mathrm{Re}_p + 0.48\,\mathrm{Re}_p^{1/2})}{1 + 0.03\,\mathrm{Re}_p + 0.48\,\mathrm{Re}_p^{1/2}} + 0.1Ma_p^2 + 0.2Ma_p^8\right] + & \\ 0.6(\gamma/2)^{1/2}Ma_p\left[1 - \exp\left(-\dfrac{Ma_p}{\mathrm{Re}_p}\right)\right] & \text{for } Ma_p <= 1 \\ \dfrac{0.9 + \dfrac{0.34}{Ma_p^2} + 1.86\left(\dfrac{Ma_p}{\mathrm{Re}_p}\right)^{1/2}\left[2 + \dfrac{4}{\gamma Ma_p^2} + 1.058\,\dfrac{1}{Ma^p}\left(\dfrac{2T_p}{\gamma T}\right)^{1/2} - \dfrac{4}{\gamma^2 Ma_p^4}\right]}{1 + 1.866(Ma_p/\mathrm{Re}_p)^{1.2}} & \text{for } Ma_p >= 1.75 \\ C_D(1.0, \mathrm{Re}_p) + (4/3)(Ma_p - 1)[C_D(1.75, \mathrm{Re}_p) - C_D(1.0, \mathrm{Re}_p)] & \text{for } 1 < Ma_p < 1.75 \end{cases} \qquad \text{(Eq 5)}$$

where Ma_p, Re_p, and T_p are particle Mach number, particle Reynolds number, and particle temperature, respectively. T and γ are gas temperature and specific heat ratio. A separate user defined function was written to calculate the C_D.

2.3 Boundary Conditions

Boundary condition and computational domain for the simulation is as shown in Fig. 3. The computational domain is only a slice with an azimuthal angle of 6 degrees. There are three inlets and the mass flow rates used in the simulation are given in Table 2. All gas inlet temperatures are assumed to be at 313 K. The walls are smooth and have a constant temperatures of 350 K. Pressure is assumed to be atmospheric in the far field boundary.

2.4 Numerical Technique

This work uses the Fluent version 6.1.22 computer code, which is commercially available from Fluent Inc. Technology (Lebanon, NH). A finite volume method for predicting flows at supersonic speeds is used for an axi-symmetric geometry. The primary variables are the velocity components, pressure and temperature. Density is linked to pressure via an equation of state. The computational domain is subdivided into a number of quadrilateral control volumes. Integrating the conservation laws over each control volume results in systems of nonlinear algebraic equations that are solved simultaneously. For modeling combustion, the standard eddy dissipation model (EDM) provided by Fluent is used where kinetic rate of change of any species in a reaction is described by an Arrhenius expression involving an exponential dependence on temperature and a power law dependence on the concentration species. To understand the effect of shock diamonds and bow shock the authors have simulated a supersonic flow in an axi-symmetric converging diverging nozzle, with two different sizes of particles namely 15 and 30 μm, impinging on flat, convex, and concave substrates. The particle material under study is MCrAlY with a density of 8900 kg/m^3. The substrate is located at a standoff distance of 250 mm from the nozzle exit. The flat substrate is assumed to extend up to 25 mm from the nozzle centerline, and for the concave and convex substrate the radius of curvature is 25 mm.

3. Results and Discussions

3.1 Gas Phase

The authors have presented the results obtained for the three substrate configurations with two different particle sizes. The behavior of the gas phase is first analyzed and then the trajectory of particle in the gas phase is observed and the results are discussed in the following sections.

General characteristics of the free jet and the flow for three different substrates (flat, convex, and concave) are shown in Fig. 4. The value of the Mach number at different regions can be found by comparing the numbers mentioned in the respective region. At the throat section of the nozzle, the Mach number is around 1 and as the sonic flow expands in the diverging section of the nozzle, a supersonic flow develops in this region. Finally, the high speed gas leaves the nozzle with an average Mach number of 2.3. Four or possibly five shock diamonds can be identified before the flow stabilizes to atmospheric pressure due to the fact that shocks are attenuated by turbulent shear layers. The shock diamonds are more clearly visible in Fig. 2. Furthermore, the gas flow is decelerated and diverted near the substrate. A bow shock can be observed near the substrate as a result of the jet impingement on the wall. It is evident from these results that the flow regime is changed significantly near the substrate due to the gas flow impingement on the wall. More importantly, variation of the flow regime is strongly dependent on the shape of the substrate. Resolving the supersonic flow and its interaction with the coating particles in this critical region (i.e., near the substrate) is eminent to predict particle conditions such as particle trajectory, velocity, and temperature upon impact.

3.1.2 Particle Phase

The MCrAlY particles are injected in the nozzle's particle inlet. The particles accelerate in the downstream along with the

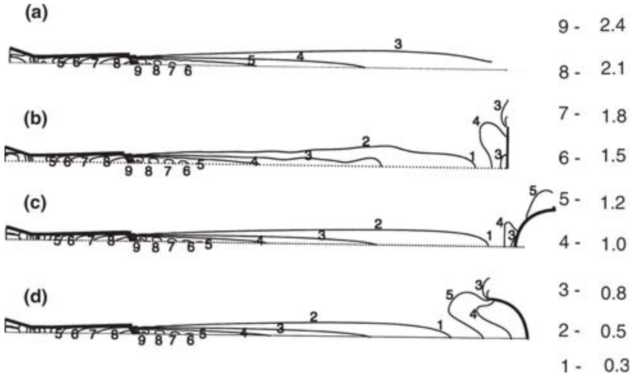

Fig. 4 Gas Mach number contours: (a) free jet, (b) flat, (c) convex, and (d) concave substrates

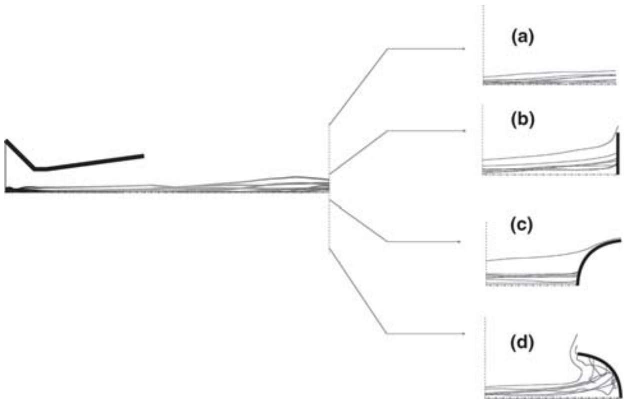

Fig. 5 Trajectory of 15 μm particles (a) in a free flow, (b) flat substrate, (c) convex, and (d) concave substrate. (The figure is enlarged three times near the substrate.)

Table 3 The 15 μm particle conditions at nozzle exit plane and imaginary plane at 250 mm from the nozzle exit in a free jet

Axial location	Average location from centerline, mm	Std deviation, mm	Average velocity, m/s	Std deviation, m/s
Nozzle exit, 0 mm	0.91	0.05	1122.20	30.20
Plane at 250 mm	5.15	2.88	310.95	32.41

Table 4 The 30 μm particle conditions at nozzle exit plane and imaginary plane at 250 mm from the nozzle exit in a free jet

Axial location	Average location from centerline, mm	Std deviation, mm	Average velocity, m/s	Std deviation, m/s
Nozzle exit, 0 mm	0.76	1.01	486	12.72
Plane at 250 mm	1.87	0.001	436	5.80

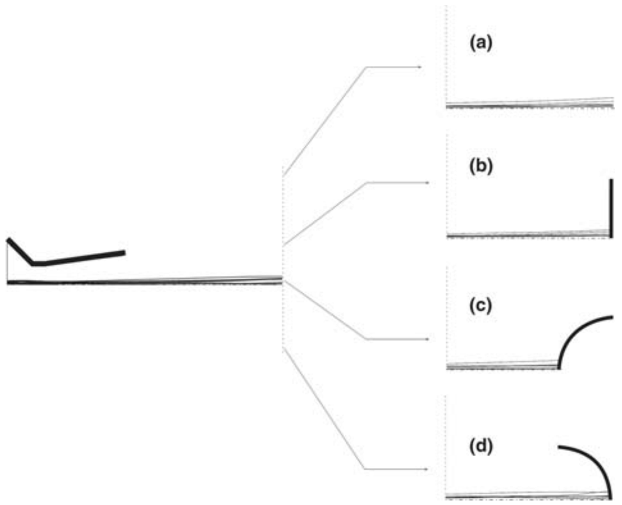

Fig. 6 Trajectory of 30 μm particles (a) in a free flow, (b) flat substrate, (c) convex, and (d) concave substrate. (The figure is enlarged three times near the substrate.)

gas. The influence of the shocks shown in Fig. 4 on the particle conditions would be a major factor that would affect deposition of the coating particles. Hence, the particle-shock interactions are studied and discussed in this section. Figure 5 shows trajectories of 15 μm particles impinging on the flat, concave, and convex substrates. As shown in Fig. 5, it is observed that the trajectory of particles abruptly change after they pass the shock diamonds and bow shock near the substrate. The trajectory of the particle is the same before a short distance from the substrate, irrespective of the configuration of substrate. However, the trajectory of particles changes as they come close to the substrate, due to the bow shock present on the substrate. Some particle streams escape without even landing on the substrate. This demonstrates that the bow shock is so strong that few particles with low velocity are not able to penetrate the shock zone. The behavior of particles is different for different substrates. Figure 6 shows the trajectory of 30 μm particles impinging on the flat, convex, and concave substrates. It is evident that the 30 μm particles that are heavier than the 15 μm particles are least affected either by the shock diamonds or the bow shocks that are present near the substrate.

To thoroughly understand the behavior of particles as they interact with the shocks, it is necessary to investigate the average location of particles off the nozzle centerline. To understand the effect of shock diamonds on particle trajectory, the behavior of particles in a free jet flow, which is not obstructed by any substrate, is studied. Tables 3 and 4, show the average location of particles off the centerline, the average axial velocity and standard deviation at the nozzle exit (i.e., before it encounters shock diamonds) and near the substrate (i.e., after it encounters the shock diamonds) for particles of size 15 and 30 μm. Tables 3 and 4 show the average location of particles of 15 μm size and that of 30 μm, respectively, are more or less close to each other before they encounter the shock diamonds. The axial velocities of 30 μm particles which are less than that of 15 μm particles can be attributed to their heavier size and consequently larger Stokes number (Ref 8) which is defined as ratio of particle response time to a time characteristic of the fluid motion.

From the previously referenced table it is evident that the trajectory and velocity of 15 μm particles are severely affected when they pass through the shock diamonds, whereas the change in particle conditions for 30 μm particles are not very significant as they are very large in size and mass when compared with 15 μm particles.

To understand the effect of bow shock on particle conditions, the average location of the particles and their normal velocity at a standoff distance of 250 mm from the nozzle exit with and without a substrate are compared and the results are shown in Fig. 7(a), (b), 8(a), and (b). The shaded region in the figure is the region within which a particle would land on the substrate. Any particle whose landing location is outside this shaded region will not land on the substrate.

The effect of bow shock on the particle trajectory is very evident from Fig. 8(a) where a lot of particles are escaping due to the fact they cannot penetrate the strong bow shock near the substrate. This effect can be understood by comparing Fig. 7(a) with

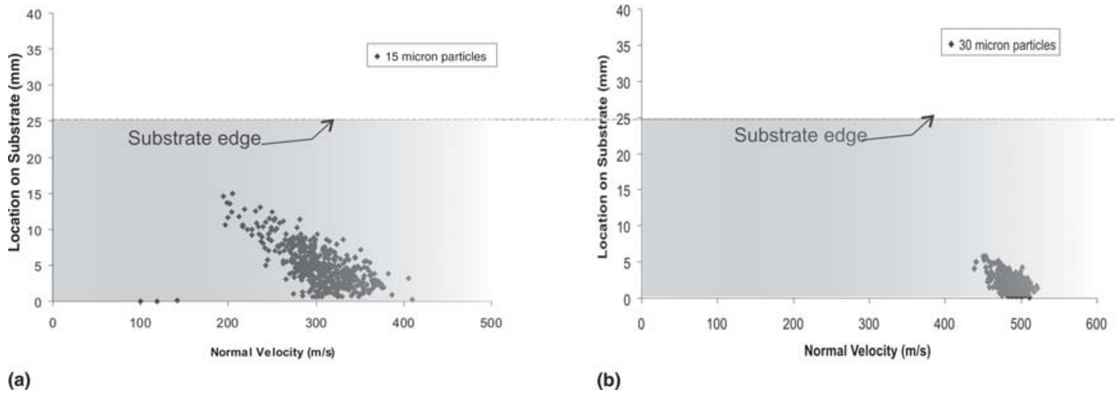

Fig. 7 Axial velocity and special distribution for (a) 15 μm particle and (b) 30 μm particles in a free jet incident on a plane 250 mm from the nozzle exit

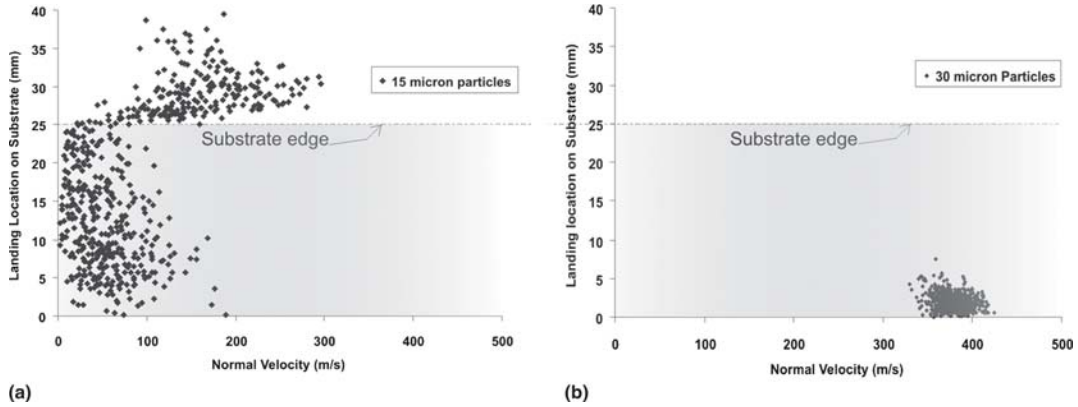

Fig. 8 Axial velocity and spatial distribution on a flat substrate kept at standoff distance 250 mm for (a) 15 μm particle (b) 30 μm particle

8(a). It is interesting to see that both the landing location and average velocity of impact has not changed significantly for 30 μm particles. They are more or less the same for both free jet and flow with a substrate. Particle conditions impinging on a flat substrate is illustrated clearly in Table 5. The mean particle landing position for 15 μm is around 18.5 mm off the centerline and its standard deviation is 10.01 mm, which implies that particles may land 10 mm on either side of the mean. This implies that many particles may escape without landing on the substrate, if their size is small. In fact, it was observed that of 1000 particles fed around 300–400 particles escape without landing on the substrate. The mean landing position for 30 μm particles is 1.97 mm off the centerline, which is very close to the centerline and their standard deviation is 1.07 mm from the mean. This proves that all of the 30 μm particles fed would land on the substrate. The average impact velocity for 30 μm particles is 375 m/s, which is higher than that of 15 μm particles. From this analysis it is observed that the presence of substrate in the flow regimen gives raise to bow shocks, which deviates the lighter particles away from their trajectory.

It will be interesting to see the effect of bow shock on particle trajectory when it is formed on different substrate configurations. When the particle impinges on a flat substrate, the axial velocity of particle becomes its velocity of impact. However, when a particle impinges on a curved substrate then the velocity of impact will be the normal velocity of particle at which it impinges. To study the effect of substrate configuration on particle conditions flat, convex, and concave substrates of 25 mm radius are used. The normal velocity of impact is a very critical factor that decides the particle landing on the substrate.

Table 5 Particle conditions before impact on a flat substrate

Particle size, μm	Average landing location, mm	Std deviation	Average velocity, m/s	Std deviation
15	18.45	10.01	93.95	66.65
30	1.97	1.07	375.52	16.27

Figures 8, 9, and 10 demonstrate the distribution of particles and their normal velocity when they impinge on various substrate configurations. The average landing position and velocity of impact are different for different substrate configuration. There are some particles that do not hit the substrate. This is because the 15 μm particles are easily flushed away by the gas phase near the substrate. It is very crucial to look at the mean landing location and mean normal velocity of impact of 15 μm particles impacting on three different substrate configurations.

Table 6 shows the mean location of landing and mean normal velocity and their standard deviation for two different sizes of

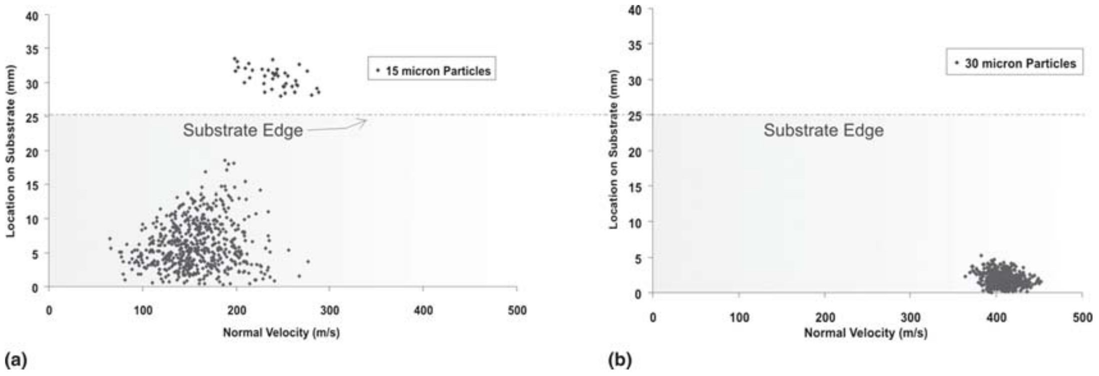

Fig. 9 Axial velocity and spatial distribution on a convex substrate kept at stand-off distance 250 mm for (a) 15 μm particle (b) 30 μm particle

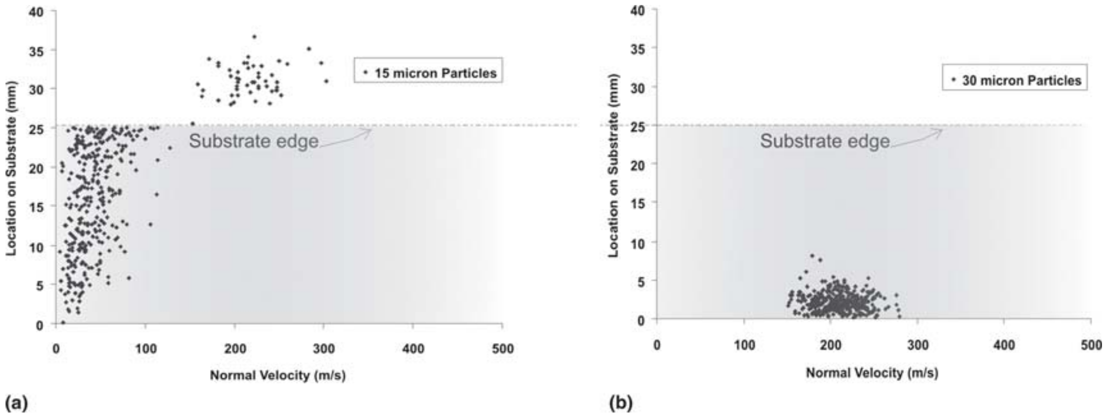

Fig. 10 Axial velocity and spatial distribution on a concave substrate kept at standoff distance 250 mm for (a) 15 μm particle (b) 30 μm particle

particles impinging on a convex substrate. For the 15 μm particles, the mean landing location is 7.84 mm off the nozzle centerline and standard deviation is around 7 mm. The normal velocity of impact is 162 m/s and the standard deviation is 39.68 m/s. This indicates that the deviation from the nozzle centerline is very low when compared with a flat substrate (Table 4), whereas for a 30 μm particle, the mean landing location and normal velocity of impact is more or less the same for both flat and convex substrates.

Table 7 shows the particle conditions impacting on a concave substrate. The mean landing position is 17.68 mm off the nozzle centerline. This large deviation from the centerline is due to the strong bow shock formed on the substrate. This bow shock is stronger than the bow shock formed on the convex substrate. This can be understood by comparing the mean landing locations of particle impinging on convex and concave substrates. Tables 6 and 7 show that the deviation of 15 μm particle impinging on a concave substrate is more than that of the same particles impinging on a convex substrate. This strong bow shock decelerates the flow largely, and consequently the normal velocity of particles hitting on the substrate becomes very low. Although the mean landing location for 30 μm particle is comparable to that of a 30 μm impinging on a convex substrate, their normal velocity is very low and the standard deviation from the mean is very high. This is due to the strong bow shock formed on the concave substrate.

Table 6 Particle conditions before impact on a convex substrate

Particle size, μm	Average landing location, mm	Std deviation, mm	Average velocity, m/s	Std deviation, m/s
15	7.84	7.02	162.52	39.68
30	1.77	0.92	480.65	14.63

Table 7 Particle conditions before impact on a concave substrate

Particle size, μm	Average landing location, mm	Std deviation, mm	Average velocity, m/s	Std deviation, m/s
15	17.68	8.22	76.37	62.40
30	2.14	1.20	210.59	24.66

4. Conclusions

The supersonic flow with particles impinging on three different substrates is simulated. The effects of shock diamonds and bow shocks on the surface of the substrate on two different particle sizes namely 15 and 30 μm are analyzed. It was found that 15 μm particles being very light are largely affected by the shock diamonds at the nozzle exit and bow shock near the substrate, whereas 30 μm particles are least affected by either shock diamonds or bow shocks. This is due to larger Stokes number associated with 30 μm particles, which is the ratio of particle response time to a time characteristic of the fluid motion (Ref 8). When it comes to the choice configuration of substrate, convex substrate is better when compared with flat and concave configurations. Although the shape of the concave substrate is favorable for capturing all the particles, the strength of bow shock formed on a concave surface is very high that they deviate most of the lighter particles.

References

1. N. Sinha, B.J. York, A. Hosangadi, and S.M. Dash, First Principles-Based Computational Fluid Dynamic (CFD) Model of Thermal Spray Deposition Process. *Proceedings of the Eighth National Thermal Spray Conference,* September 11-15, 2005 (Houston, TX), p 199-206
2. X. Yang and S. Eidelman, Numerical Analysis of a High Velocity Oxygen Fuel Thermal Spray System, *J. Therm. Spray Technol.,* 1996, **5**(2), p 175-184
3. A. Dolatabadi, V. Pershin, and J. Mostaghimi, New Attachment for Controlling Gas Flow in the HVOF Process, *J. Therm. Spray Technol.,* 2005, **14**(1), p 91-99
4. A. Dolatabadi, J. Mostaghimi, and V. Pershin, Effect of Cylindrical Shroud on Particle in High Velocity Oxy-Fuel Spray Process, *Sci. Technol. Adv. Mater.,* 2002, **3,** p 245-255
5. B.E. Launder and D.B. Spalding, The Numerical Calculation of Turbulent Flows, *Comp. Meth. Appl. Mech. Eng.,* 1974, **3,** p 269-289
6. C. Crowe and D. Stock, A Computer Solution for Two-Dimensional Fluid–Particle Flows, *Int. J. Numer. Methods Eng.,* 1976, **19,** p 185-196
7. C.B. Henderson, Drag Coefficient of Spheres in Continuum and Rarefied Flows, *AIAA Journal,* 1976, **14**(6), p 707-708
8. C.T. Crowe, T.R. Troutt, and T.J. Chung, Num. Models for Two-Phase Turbulent Flows, *Ann. Rev. Fluid Mech.,* 1996, **28,** p 11-43